Three-dimensional spatially localized binary-fluid convection in a porous medium

David Lo Jacono[1,†], Alain Bergeon[1] and Edgar Knobloch[2]

[1]Institut de Mécanique des Fluides de Toulouse (IMFT), CNRS, UPS, Université de Toulouse,
Allée Camille Soula, F-31400 Toulouse, France
[2]Department of Physics, University of California, Berkeley, CA 94720, USA

Three-dimensional convection in a binary mixture in a porous medium heated from below is studied. For negative separation ratios steady spatially localized convection patterns are expected. Such patterns, spatially localized in two dimensions, are computed and numerical continuation is used to examine their growth and proliferation as parameters are varied. The patterns studied have the form of a core region with four extended side-branches and can be stable. A physical mechanism behind the formation of these unusual structures is suggested.

Key words: convection, convection in porous media, nonlinear dynamical systems

1. Introduction

Stationary spatially localized states are of great interest in the theory of pattern formation. Recently two-dimensional states of this type, localized in one dimension, have been found in several different types of convection, including binary-fluid convection (Batiste & Knobloch 2005; Batiste *et al.* 2006), convection in an imposed magnetic field (Blanchflower 1999; Lo Jacono, Bergeon & Knobloch 2011) and natural doubly diffusive convection (Ghorayeb & Mojtabi 1997; Bergeon & Knobloch 2008; Bergeon *et al.* 2008). Similar states, localized in the cross-stream direction, have been identified in plane Couette flow (Schneider, Gibson & Burke 2010*a*). In these systems, localized states occur inside the region of coexistence between a spatially homogeneous state and a spatially periodic state, in a parameter interval called the snaking or pinning region (Burke & Knobloch 2007). This region also contains multipulse states resembling bound states of single-pulse localized states, as demonstrated recently in the context of binary-fluid convection with a negative separation ratio (Lo Jacono, Bergeon & Knobloch 2010; Mercader *et al.* 2011). The $(1 + 1)$-dimensional Swift–Hohenberg equation provides a convenient model equation

that sheds much light on the origin and properties of the pinning region in these systems (Burke & Knobloch 2007).

It is natural to consider the existence of three-dimensional structures that are localized in *two* spatial dimensions. Structures of this type were originally found in magnetoconvection (Blanchflower & Weiss 2002) but attempts to find stable states of this type in binary-fluid convection failed, although meandering structures with slow but complex time-dependence were identified (Alonso *et al.* 2007). Related but highly anisotropic structures resembling turbulent puffs were recently computed for plane Couette flow (Duguet, Schlatter & Henningson 2009; Schneider, Marinc & Eckhardt 2010*b*). However, the Swift–Hohenberg equation (hereafter SH23 or SH35, depending on the nonlinear terms (Burke & Knobloch 2007)) does not suffer from these difficulties. This equation has variational structure in any number of dimensions and consequently evolves to steady states corresponding to local minima of the free energy. In $2 + 1$ dimensions these minima may correspond to structures that are fully localized in two dimensions (Lloyd *et al.* 2008; Avitabile *et al.* 2010). These structures can take the form of spatially localized patches of hexagons or spatially localized patches of rolls that have been called 'worms', depending on the symmetry properties of the nonlinear terms (Lloyd *et al.* 2008; Avitabile *et al.* 2010). Localized target patterns can also be found as can localized spots. Of these the hexagons, worms and targets are all found in the subcritical regime where a periodic pattern, be it hexagons or rolls, coexists with the trivial solution. As in one dimension, all these patterns 'snake', at least initially, as the structure is followed in parameter space and grows by nucleating additional cells or rings along its periphery (Lloyd *et al.* 2008; Lloyd & Sandstede 2009). Spot-like states differ in that they are present even in the supercritical regime (Lloyd & Sandstede 2009), and related states have been observed in non-variational systems, such as reaction–diffusion equations (Coullet, Riera & Tresser 2000) or the equations arising in nonlinear optics (McSloy *et al.* 2002; Vladimirov *et al.* 2002), as well as in ferrofluids (Richter & Barashenkov 2005) and an optical light valve experiment (Bortolozzo, Clerc & Residori 2009).

In this paper we select binary convection in a porous medium to study three-dimensional localized structures and their growth properties. For this purpose the mixture is required to have a negative separation ratio. The resulting system is convenient for a study of this complexity since the Darcy equation of motion determines the flow instantaneously in terms of the contributions to the buoyancy force. The dimensionless equations describing this system are

$$\boldsymbol{u} = -\nabla p + Ra(T + SC)\boldsymbol{e}_z, \quad \nabla \cdot \boldsymbol{u} = 0, \tag{1.1}$$

$$\frac{\partial T}{\partial t} = -(\boldsymbol{u} \cdot \nabla)T + \nabla^2 T, \tag{1.2}$$

$$\epsilon \frac{\partial C}{\partial t} = -(\boldsymbol{u} \cdot \nabla)C + \tau \nabla^2(C - T), \tag{1.3}$$

where $\boldsymbol{u} = (u, v, w)$ and $\nabla \equiv (\partial_x, \partial_y, \partial_z)$ in (x, y, z) coordinates, with (x, y) in the horizontal direction and z in the vertical; T is the temperature and C is the concentration of the heavier component of the mixture. The (inverse) Lewis number τ, the Rayleigh number Ra and the separation ratio S are defined by

$$\tau = \frac{D}{\kappa}, \quad Ra = \frac{g|\rho_T|\Delta Th}{\lambda \kappa}, \quad S = -S_{Soret}\frac{\rho_C}{\rho_T} < 0, \tag{1.4}$$

where λ is the Darcy friction coefficient, κ is the thermal diffusivity, D is the solute diffusivity, $S_{Soret} < 0$ is the Soret coefficient, g is the gravitational acceleration and h is the depth of the layer. The parameter ϵ denotes the porosity. In writing these equations we have used the layer depth h as a unit of length and the vertical thermal diffusion time h^2/κ as the unit of time, together with the linearized equation of state, $\rho(T, C) = \rho_0 + \rho_T(T - T_0) + \rho_C(C - C_0)$, where $\rho_T < 0$, $\rho_C > 0$ and the subscript zero indicates reference values. We suppose that a temperature difference $\Delta T > 0$ is imposed across the system with the lower boundary hotter than the upper boundary; in response the system develops a concentration difference $\Delta C = |S|\Delta T$ with C larger at the bottom than at the top. We use ΔT and ΔC as units of temperature and concentration.

Since the mass flux is proportional to the gradient of $C - T$ the boundary conditions read

$$\text{at } z = 0 : w = T - 1 = (C - T)_z = 0, \quad \text{at } z = 1 : w = T = (C - T)_z = 0, \quad (1.5)$$

together with periodic boundary conditions with dimensionless period Γ in the (x, y) directions. Note that because of the Darcy friction law we cannot impose boundary conditions on (u, v) at $z = 0, 1$. Thus the velocity boundary conditions are 'stress-free'. This property of the system is beneficial for numerical continuation; the absence of nonlinear terms in the equation of motion (the effective Prandtl number in the medium is infinite) also helps.

In the following we write $T = 1 - z + \Theta$, $C = 1 - z + \Sigma$ and examine the properties of the equations for u, v, w, Θ and Σ, all of which vanish in the conduction state. These equations are equivariant under translations in (x, y) modulo the period Γ. In addition, they are equivariant under the reflection $(x, y) \rightarrow (-x, y)$ and the 90° rotation $(x, y) \rightarrow (-y, x)$. Together these symmetries generate the symmetry group $D_4 \dot{+} T^2$, where D_4 is the symmetry of a square, T^2 denotes a two-torus of translations and the symbol $\dot{+}$ indicates the semidirect product (Silber & Knobloch 1988). Finally, with the boundary conditions (1.5) the equations are also equivariant with respect to the midplane reflection $z \rightarrow 1 - z$. The latter symmetry favours roll-like patterns (Golubitsky, Swift & Knobloch 1984; Umla *et al.* 2010) and therefore plays an essential role in the observed patterns.

We solve (1.1)–(1.3) with the boundary conditions (1.5) on a square domain of size $\Gamma = 18\lambda_c \times 18\lambda_c$ where λ_c denotes the critical wavelength at onset of steady-state instability (we use $\lambda_c = 2\pi/k_c$ with $k_c = 3.75$, as appropriate for the representative parameter values $\epsilon = 1$, $\tau = 0.5$, $S = -0.1$ employed below). We use numerical continuation to follow steady states from small-amplitude states present close to the primary instability. The spectral element method used favours solutions with square symmetry close to onset (Assemat, Bergeon & Knobloch 2007). There are two types of such solutions, both invariant with respect to the pair of reflections $(x, y) \rightarrow (-x, y)$ and $(x, y) \rightarrow (x, -y)$. The first is also invariant with respect to reflections in the diagonal, $(x, y) \rightarrow (y, x)$, and is therefore D_4-symmetric. The second breaks the symmetry $(x, y) \rightarrow (y, x)$ and is therefore D_2-symmetric (more precisely, $D_2 \times Z_2$-symmetric, where the symmetry Z_2 refers to reflection in the midplane). In the following we refer to the former as even and the latter as odd (based on their symmetry with respect to the diagonal) and use red and black colours to distinguish between them in the bifurcation diagrams that follow. Because of the above symmetries all our calculations are performed in a quarter-domain of size $9\lambda_c \times 9\lambda_c$ and then reflected appropriately in the axes to generate a structure with four-fold symmetry. The continuation method used is described by Lo Jacono *et al.* (2010) but
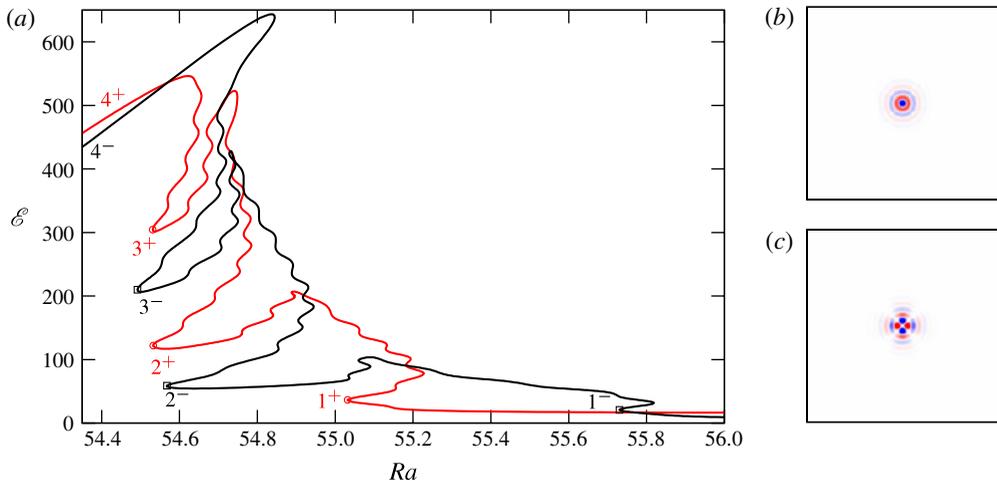
FIGURE 1. (*a*) Bifurcation diagram showing the kinetic energy $\mathscr{E}$ as a function of the Rayleigh number Ra for D_4-symmetric solutions (red curve) and D_2-symmetric solutions (black curve), showing snaking behaviour associated with growth of the nucleus (large excursions) with small superposed oscillations associated with the growth of the arms via nucleation of new rolls at the tip. (*b,c*) Localized states along the branch of D_4-symmetric solutions (*b*) and D_2-symmetric solutions (*c*) at $Ra = 60.66783$ and $Ra = 60.61625$, respectively.

employs three-dimensional spectral element spatial discretization similar to that used by Assemat *et al.* (2007), and takes advantage of full tensorization of the Helmholtz and Poisson operators in the three spatial directions. We mention that periodic D_4- and D_2-symmetric states both set in at $Ra = Ra_c \approx 66.657$. This critical value is smaller than the critical Rayleigh number for the onset of convection in two dimensions, $Ra_c \approx 66.75$ (Lo Jacono *et al.* 2010), i.e. for the appearance of straight rolls. As in two dimensions the three-dimensional localized states are created in secondary bifurcations from these periodic states (not shown).

2. Results

Figure 1(*a*) shows the resulting bifurcation diagram. It shows the volume integral of the kinetic energy, $\mathscr{E}$, for the even and odd states as a function of the Rayleigh number Ra. The continuation shows that close to onset the D_4-symmetric spatially extended eigenfunction present at $Ra = 66.657$ self-localizes into a target pattern. Figure 1(*b*) shows such a pattern at $Ra = 60.66783$. When this state is continued to smaller values of Ra it becomes more and more localized but by $Ra = 56.25$ the circular symmetry of the pattern is conspicuously broken, resulting in a finger-like state with D_4 symmetry. Figure 2(*a*) shows the subsequent evolution of this state in terms of the midplane vertical velocity $w(x, y, z = 1/2)$ at successive left saddle-nodes (folds) of the red branch in figure 1(*a*). The figure reveals a broad pattern: the large excursions in the branch correspond to mergers of the rolls at the base of each finger into successive concentric rings around the centre of the structure. In contrast, the smaller wiggles along the branch correspond to the nucleation of new rolls at the tips of the fingers. Thus the large excursions are associated with the growth of the core or nucleus of the structure while the small oscillations reflect the elongation of the arms.
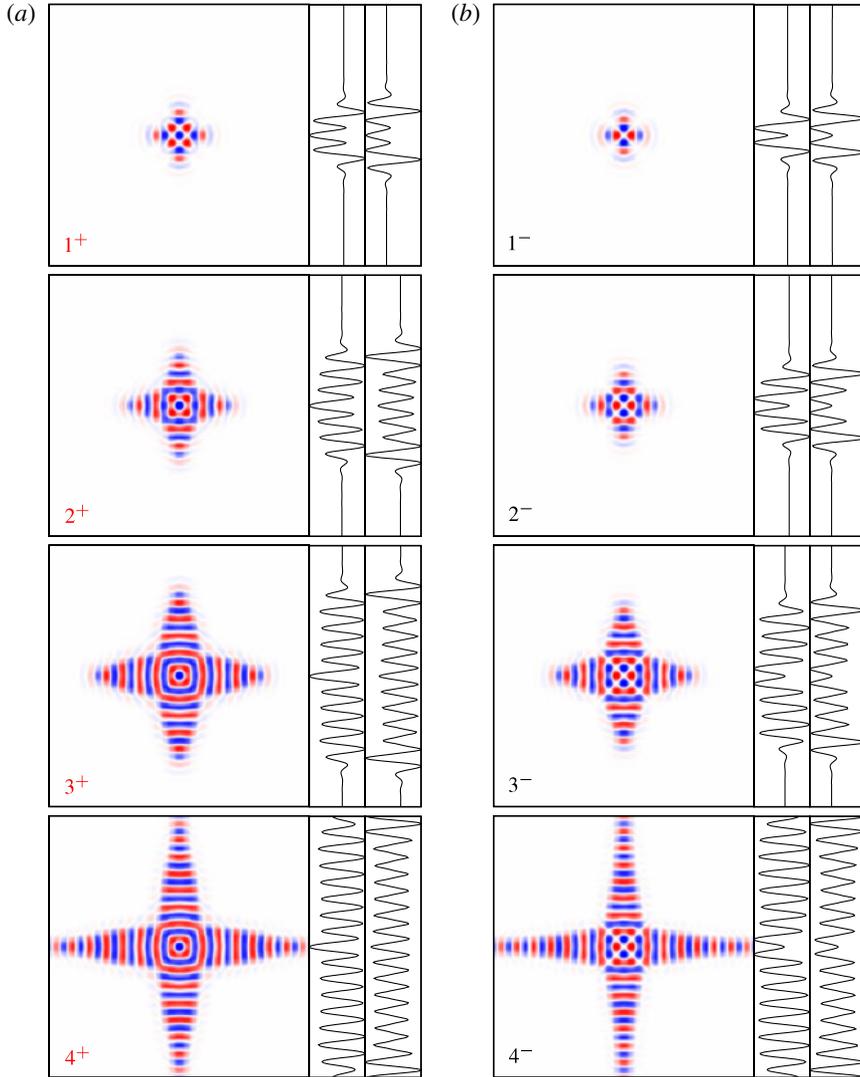
FIGURE 2. The vertical velocity $w(x, y, 1/2)$ in the layer midplane at the four leftmost saddle-nodes on the branch of (a) the D_4-symmetric solutions, and (b) the D_2-symmetric solutions. Red (blue) indicates upward (downward) flow. The figures are labelled following the saddle-node labels in figure 1. The sidepanels show $\Theta(0, y, 1/2)$ (left plots) and $\Sigma(0, y, 1/2)$ (right plots) both scaled to lie between ± 1.

Beyond the region shown the structure becomes so large that it reaches the domain boundary and interacts with its mirror images. At this point the structure stops being fully localized and the subsequent behaviour of the solution branch is dominated by the interaction with adjacent structures (not shown).

Figure 1(c) shows a different type of target-like structure obtained at $Ra = 60.61625$ from the D_2-symmetric eigenfunction at $Ra_c \approx 66.657$. This solution is strongly spatially localized but D_2-symmetric. As one follows this state to larger amplitude (black curve in figure 1a) it sends out four arms in the principal directions (figure 2b). Once again the large excursions reflect the growth of the nucleus of the structure while
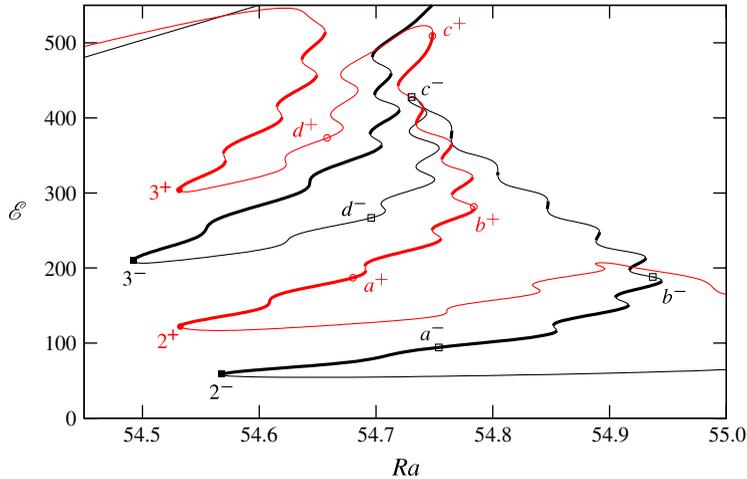
FIGURE 3. Detail of the central portion of figure 1. Heavy (light) line segments indicate stable (unstable) solutions.

the smaller oscillations superposed on them are a consequence of the nucleation of additional rolls at the tips of the four arms whereby the arms elongate.

It is noteworthy that in both cases the solution branches do not grow monotonically in amplitude. Thus some of the small oscillations correspond to the nucleation of new rolls while others reflect roll destruction. In addition, while the large excursions governing the growth of the core are more or less vertically aligned as expected of homoclinic snaking of target-like structures in simpler systems (Lloyd & Sandstede 2009) the small superposed oscillations are not (figure 3). This is indicative of the fact that the nucleus and the arms tend to grow simultaneously. We also note that the amplitude of the solutions at the folds of the large excursions is generally substantially lower on the left than further to the right. This is a consequence of strong Ra-dependent wavelength selection: the wavelength along the arms shrinks as Ra decreases, leading to a shrinkage of the arms (including the elimination of some rolls at the tips; these rolls are restored above the leftmost folds as the arms start to grow again and the wavelength increases). Figure 4 shows this process in greater detail. The figure shows a series of snapshots of the midplane vertical velocity $w(x, y, z = 1/2)$ along the portion of the D_4-symmetric branch (figure 4a) and the D_2-symmetric branch (figure 4b) between the second and third leftmost folds on these branches at the locations indicated in figure 3. A careful examination shows that both localized states add a central ring during this process, while the arms initially grow by adding rolls and then shrink again. However, despite the incorporation of the rolls at the base of each arm into the nucleus, at the end of this process both arms are longer than at the beginning. Moreover, as a consequence of the Ra-dependence of the wavelength the arms at the left saddle-node are long and skinny while those at the next saddle-node on the right are relatively short and fat.

Each arm of the localized state individually resembles a state that has been called a 'worm', i.e. a roll-like structure, spatially localized in two dimensions (Joets & Ribotta 1988; Dennin, Ahlers & Cannell 1996). Related states have also been seen in the Faraday instability in domains with flexible boundaries (Pucci *et al.* 2011). Although stationary solutions of this type occur in simple variational models such as SH35 in $2 + 1$ dimensions (Avitabile *et al.* 2010) the appearance of strongly non-convex
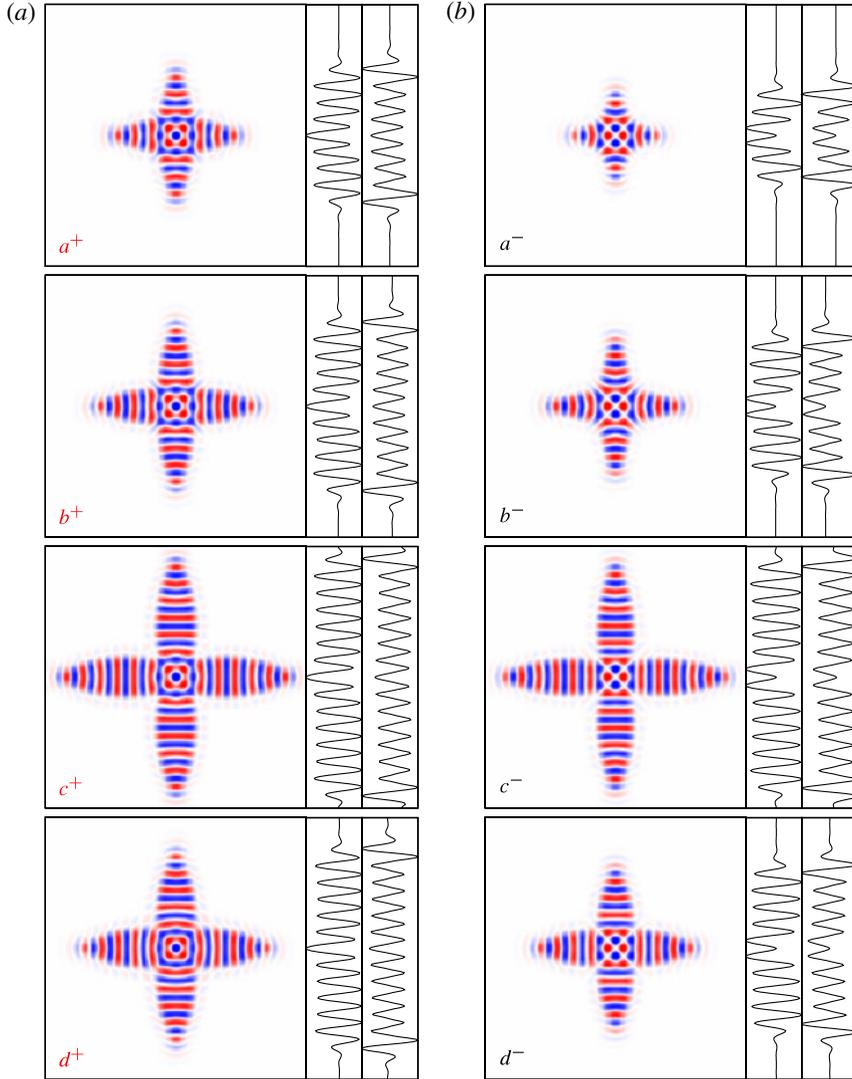
FIGURE 4. As for figure 2 but showing the midplane vertical velocity $w(x, y, 1/2)$ at four locations between the second and third leftmost saddle-nodes on the branch of (a) D_4-symmetric solutions, and (b) D_2-symmetric solutions, labelled as in figure 3. The sidepanels show $\Theta(0, y, 1/2)$ (left plots) and $\Sigma(0, y, 1/2)$ (right plots) both scaled to lie between ± 1.

structures such as those found here demands explanation. For this purpose we show alongside each planform the profiles of the midplane temperature $\Theta(0, y, 1/2)$ (left sidepanels) and concentration $\Sigma(0, y, 1/2)$ (right sidepanels) along the $x = 0$ slice. The concentration profiles demonstrate that in the present system the growth of the arms in the longitudinal direction is opposed not only by the pinning of the advancing front to the rolls behind it (as occurs, for example, in the two-dimensional SH35 (Avitabile *et al.* 2010)) but in addition by the concentration bump generated in front of the arms by longitudinal pumping of concentration (Mercader *et al.* 2009). The localization in the transverse direction is more subtle since here the front is (almost) parallel to the
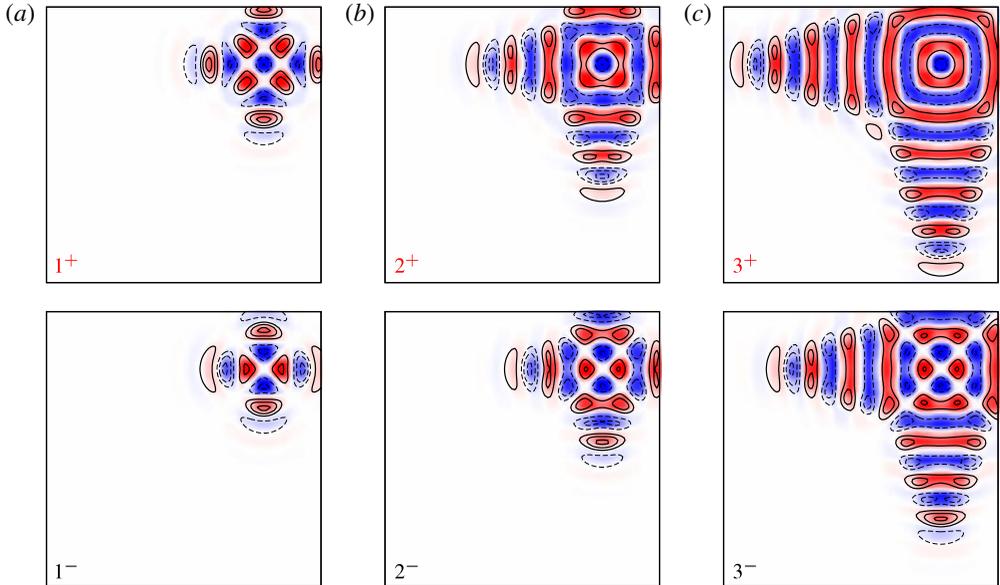
FIGURE 5. The midplane vertical velocity $w(x, y, z = 1/2)$ and line contours of the concentration $\Sigma(x, y, z = 1/2)$ for even and odd solutions at the locations $1^\pm$, $2^\pm$ and $3^\pm$ in figure 1. Red (blue) indicates upward (downward) flow. Only part of the domain is shown.

roll wavevector and pinning is dramatically reduced. Nonetheless, studies of SH35 reveal that stationary worms do localize in this direction as well, and Avitabile *et al.* (2010) conjecture that this is due to the wavenumber gradient near the boundary of the structure. However, in the present case the concentration field again plays an essential role. Figure 5 shows contours of constant concentration superposed on the midplane vertical velocity. The figure reveals that the concentration (and temperature) are in phase in the nucleus and along the centreline of each arm: rising flow carries higher concentration (and temperature) upwards. However, the figure also reveals that along the lateral boundary of each arm the expulsion of concentration from the structure generates a concentration 'moat' that traps the structure, much as occurs in one spatial dimension (Riecke 1992; Alonso *et al.* 2010). We believe that this is the fundamental reason why binary-fluid convection in a porous medium generates the remarkable spatially localized structures shown in the preceding figures.

In order to determine the stability properties of the solutions we have found we solved the linear stability problem in the quarter-domain with imposed symmetry (antisymmetry) in the diagonal as appropriate. The results are in all cases in agreement with the intuition developed from SH35. Specifically, every segment in figure 3 with positive slope corresponds to stable solutions (heavy line segments) with the remaining solutions unstable (thin line segments). The midplane reflection symmetry plays an important role in these stability results; without it the rolls are unstable to hexagonal structures as described by SH23. In bulk binary mixtures, in contrast, no stable spatially localized two-dimensional stationary states have hitherto been found (Alonso *et al.* 2007). We have not examined the stability of the structures with respect to infinitesimal perturbations on larger domains or with respect to asymmetric or finite-amplitude perturbations.
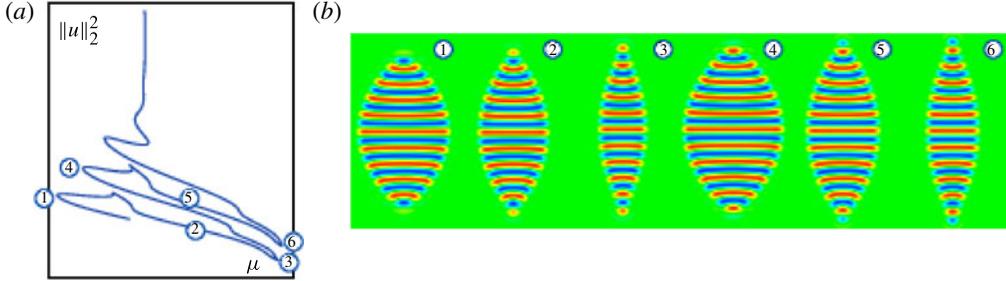
FIGURE 6. Continuation of time-independent worms in SH35 with $b_3 = 2.46$ reveals that the curvature of the worm boundary near its tips changes along the solution branch: the sign of the curvature of the localized patterns in panels 3 and 6 near the tips differs from those in the other panels. From Avitabile *et al.* (2010).

3. Discussion

From the above pictures we abstract two basic principles. The localized structure grows continuously in area, with qualitative changes in the bifurcation diagram associated with interactions with the domain. However, the amplitude of the solution, here measured by the total kinetic energy $\mathcal{E}$, does not increase monotonically. This is because the arms of the structure shrink transversally as the Rayleigh number decreases and swell as it increases. Indeed, we find that for $Ra \lesssim 54.6$ the arms thin with distance from the core but thicken with distance for $Ra \gtrsim 54.6$, with $Ra \approx 54.6$ playing the role of a Maxwell point at which the energy along the arms of the structure is independent of the distance from the core. Similar behaviour is also observed in individual worms as described by the Swift–Hohenberg equation SH35,

$$u_t = -\mu u - (\nabla^2 + 1)^2 u + b_3 u^3 - u^5, \qquad (3.1)$$

where b_3 is a positive constant that determines the extent of bistability between the trivial state $u = 0$ representing the conduction state and a periodic state $u(x, y)$, here a roll pattern, representing convection. The symmetry $u \rightarrow -u$ of (3.1) plays the role of the midplane reflection symmetry of (1.1)–(1.3) when the boundary conditions (1.5) are used. Equation (3.1) exhibits worm-like states that are fully localized in two spatial dimensions; these worms snake when continued in μ, at least initially, where μ is to be identified with $Ra_c - Ra$. Moreover, multiple disconnected branches of worms are present (Avitabile *et al.* 2010). Figure 6, a reproduction of figure 33 from Avitabile *et al.* (2010), reveals a strong selection between skinny worms at the right of the snaking region (larger μ) and pudgy worms at the left of the snaking region (smaller μ). Additional rolls start to nucleate in the middle of the associated snaking region and do so simultaneously at both tips (head and tail) of the worm. The increased radius of curvature of the worm demands a smaller wavenumber along the periphery and this change of wavenumber is enough to pin the front between the roll state and the homogeneous state and maintain a steady state. Note that the worm-like appendages at the right of the pinning region are concave near the tip implying that they are confined by more than surface energy, i.e. both the curvature of the rolls inside the structure and the wavenumber along the periphery determine jointly the pinning of the bounding fronts to the roll structure within. In contrast, the worms at the left edge of the pinning region are convex and look as if they are held together by an

effective surface tension. The solutions described in the present paper share some of the properties of these worm states but the growth of the highly non-convex arms appears to be a consequence of localization by the expelled concentration field. This localization process is somewhat similar to that leading to localized structures in phase field crystal models where the growth of the solid phase uses up nearby 'mass' thereby stabilizing the structure (Tegze *et al.* 2011); finger-like states are favoured since new 'mass' reaches the tips of the fingers via diffusion more easily than other parts.

Acknowledgements

References

ALONSO, A., BATISTE, O., KNOBLOCH, E. & MERCADER, I. 2010 Convectons. In *Localized States in Physics: Solitons and Patterns* (ed. O. Descalzi), pp. 109–125. Springer.

ALONSO, A., BATISTE, O., MESEGUER, A. & MERCADER, I. 2007 Complex dynamical states in binary mixture convection with weak negative Soret coupling. *Phys. Rev.* E **75**, 026310-1–15.

ASSEMAT, P., BERGEON, A. & KNOBLOCH, E. 2007 Nonlinear Marangoni convection in circular and elliptical cylinders. *Phys. Fluids* **19**, 104101-1–17.

AVITABILE, D., LLOYD, D. J. B., BURKE, J., KNOBLOCH, E. & SANDSTEDE, B. 2010 To snake or not to snake in the planar Swift–Hohenberg equation. *SIAM J. Appl. Dyn. Syst.* **9**, 704–733.

BATISTE, O. & KNOBLOCH, E. 2005 Simulations of localized states of stationary convection in ^{3}He–^{4}He mixtures. *Phys. Rev. Lett.* **95**, 244501-1–4.

BATISTE, O., KNOBLOCH, E., ALONSO, A. & MERCADER, I. 2006 Spatially localized binary-fluid convection. *J. Fluid Mech.* **560**, 149–158.

BERGEON, A., BURKE, J., KNOBLOCH, E. & MERCADER, I. 2008 Eckhaus instability and homoclinic snaking. *Phys. Rev.* E **78**, 046201-1–16.

BERGEON, A. & KNOBLOCH, E. 2008 Spatially localized states in natural doubly diffusive convection. *Phys. Fluids* **20**, 034102-1–8.

BLANCHFLOWER, S. 1999 Magnetohydrodynamic convectons. *Phys. Lett.* A **261**, 74–81.

BLANCHFLOWER, S. & WEISS, N. 2002 Three-dimensional magnetohydrodynamic convectons. *Phys. Lett.* A **294**, 297–303.

BORTOLOZZO, U., CLERC, M. G. & RESIDORI, S. 2009 Solitary localized structures in a liquid crystal light-valve experiment. *New J. Phys.* **11**, 093037-1–10.

BURKE, J. & KNOBLOCH, E. 2007 Homoclinic snaking: structure and stability. *Chaos* **17**, 037102-1–15.

COULLET, P., RIERA, C. & TRESSER, C. 2000 Stable static localized structures in one dimension. *Phys. Rev. Lett.* **84**, 3069–3072.

DENNIN, M., AHLERS, G. & CANNELL, D. S. 1996 Chaotic localized states near the onset of electroconvection. *Phys. Rev. Lett.* **77**, 2475–2478.

DUGUET, Y., SCHLATTER, P. & HENNINGSON, D. S. 2009 Localized edge states in plane Couette flow. *Phys. Fluids* **21**, 111701-1–4.

GHORAYEB, K. & MOJTABI, A. 1997 Double diffusive convection in a vertical rectangular cavity. *Phys. Fluids* **9**, 2339–2348.

GOLUBITSKY, M., SWIFT, J. W. & KNOBLOCH, E. 1984 Symmetries and pattern selection in Rayleigh–Bénard convection. *Physica* D **10**, 249–276.

JOETS, A. & RIBOTTA, R. 1988 Localized time-dependent state in the convection of a nematic liquid crystal. *Phys. Rev. Lett.* **60**, 2164–2167.

LLOYD, D. J. B. & SANDSTEDE, B. 2009 Localized radial solutions of the Swift–Hohenberg equation. *Nonlinearity* **22**, 485–524.

LLOYD, D. J. B., SANDSTEDE, B., AVITABILE, D. & CHAMPNEYS, A. R. 2008 Localized hexagon patterns of the planar Swift–Hohenberg equation. *SIAM J. Appl. Dyn. Syst.* **7**, 1049–1100.

LO JACONO, D., BERGEON, A. & KNOBLOCH, E. 2010 Spatially localized binary fluid convection in a porous medium. *Phys. Fluids* **22**, 073601-1–13.

LO JACONO, D., BERGEON, A. & KNOBLOCH, E. 2011 Magnetohydrodynamic convectons. *J. Fluid Mech.* **687**, 595–605.

MCSLOY, J. M., FIRTH, W. J., HARKNESS, G. K. & OPPO, G.-L. 2002 Computationally determined existence and stability of transverse structures. II. Multipeaked cavity solitons. *Phys. Rev.* E **66**, 046606-1–8.

MERCADER, I., BATISTE, O., ALONSO, A. & KNOBLOCH, E. 2009 Localized pinning states in closed containers: homoclinic snaking without bistability. *Phys. Rev.* E **80**, 025201(R)-1–4.

MERCADER, I., BATISTE, O., ALONSO, A. & KNOBLOCH, E. 2011 Convectons, anticonvectons and multiconvectons in binary fluid convection. *J. Fluid Mech.* **667**, 586–606.

PUCCI, G., FORT, E., BEN AMAR, M. & COUDER, Y. 2011 Mutual adaptation of a Faraday instability pattern with its flexible boundaries in floating fluid drops. *Phys. Rev. Lett.* **106**, 024503-1–4.

RICHTER, R. & BARASHENKOV, I. V. 2005 Two-dimensional solitons on the surface of magnetic fluids. *Phys. Rev. Lett.* **94**, 184503-1–4.

RIECKE, H. 1992 Self-trapping of traveling-wave pulses in binary mixture convection. *Phys. Rev. Lett.* **68**, 301–304.

SCHNEIDER, T. M., GIBSON, J. F. & BURKE, J. 2010*a* Snakes and ladders: localized solutions of plane Couette flow. *Phys. Rev. Lett.* **104**, 104501-1–4.

SCHNEIDER, T. M., MARINC, D. & ECKHARDT, B. 2010*b* Localized edge states nucleate turbulence in extended plane Couette cells. *J. Fluid Mech.* **646**, 441–451.

SILBER, M. & KNOBLOCH, E. 1988 Pattern selection in steady binary-fluid convection. *Phys. Rev.* A **38**, 1468–1477.

TEGZE, G., GRÁNÁSY, L., TÓTH, G. I., DOUGLAS, J. F. & PUSZTAI, T. 2011 Tuning the structure of non-equilibrium soft materials by varying the thermodynamic driving force for crystal ordering. *Soft Matt.* **7**, 1789–1799.

UMLA, R., AUGUSTIN, M., HUKE, B. & LÜCKE, M. 2010 Roll convection of binary fluid mixtures in porous media. *J. Fluid Mech.* **649**, 165–186.

VLADIMIROV, A. G., MCSLOY, J. M., SKRYABIN, D. V. & FIRTH, W. J. 2002 Two-dimensional clusters of solitary structures in driven optical cavities. *Phys. Rev.* E **65**, 046606-1–11.